High spin structure and intruder configurations in ^{31}P

M. Ionescu-Bujor,[1] A. Iordachescu,[1] D. R. Napoli,[2] S. M. Lenzi,[3] N. Mărginean,[1,2] T. Otsuka,[4,5] Y. Utsuno,[6] R. V. Ribas,[7] M. Axiotis,[2] D. Bazzacco,[3] A. M. Bizzeti-Sona,[8] P. G. Bizzeti,[8] F. Brandolini,[3] D. Bucurescu,[1] M. A. Cardona,[9] G. de Angelis,[2] M. De Poli,[2] F. Della Vedova,[3] E. Farnea,[3] A. Gadea,[2] D. Hojman,[9] C. A. Kalfas,[10] Th. Kröll,[2] S. Lunardi,[3] T. Martínez,[2] P. Mason,[3] P. Pavan,[3] B. Quintana,[3] C. Rossi Alvarez,[3] C. A. Ur,[1,3] R. Vlastou,[11] and S. Zilio[3]

[1]*National Institute for Physics and Nuclear Engineering, Bucharest, Romania*
[2]*INFN, Laboratori Nazionali di Legnaro, Legnaro, Italy*
[3]*Dipartimento di Fisica dell'Universitá and INFN, Sezione di Padova, Padova, Italy*
[4]*Department of Physics and Center for Nuclear Study, University of Tokyo, Hongo, Tokyo 113-0033, Japan*
[5]*RIKEN, Hirosawa, Wako-shi, Saitama 351-0198, Japan*
[6]*Japan Atomic Energy Research Institute, Tokai, Japan*
[7]*Instituto de Fisica, Universidade de Sao Paolo, Sao Paolo, Brazil*
[8]*Dipartimento di Fisica dell'Universitá and INFN, Sezione di Firenze, Firenze, Italy*
[9]*Departamento de Física, CNEA, and CONICET, Buenos Aires, Argentina*
[10]*Institute of Nuclear Physics, NCSR Demokritos, Athens, Greece*
[11]*National Technical University of Athens, Athens, Greece*

(Received 26 July 2005; published 13 February 2006)

The nucleus ^{31}P has been studied in the ^{24}Mg(^{16}O,2αp) reaction with a 70-MeV ^{16}O beam. A complex level scheme extended up to spins $17/2^+$ and $15/2^-$, on positive and negative parity, respectively, has been established. Lifetimes for the new states have been investigated by the Doppler shift attenuation method. Two shell-model calculations have been performed to describe the experimental data, one by using the code ANTOINE in a valence space restricted to the *sd* shell, and the other by applying the Monte Carlo shell model in a valence space including the *sd*-*fp* shells. The latter calculation indicates that intruder excitations, involving the promotion of a $T = 0$ proton-neutron pair to the *fp* shell, play a dominant role in the structure of the positive-parity high-spin states of ^{31}P.

DOI: 10.1103/PhysRevC.73.024310 PACS number(s): 21.10.−k, 23.20.Gq, 23.20.Lv, 27.30.+t

I. INTRODUCTION

A large amount of data has been obtained over many years concerning the structure of the stable or close to stability nuclei near ^{32}S. The experimental information, obtained mainly in elastic scattering, radiative capture, and transfer reactions induced by light particles, has been intensively used to test the shell-model calculations. Energy levels up to excitations around 10 MeV have been frequently found in these nuclei; however, their spins were limited to low and medium values [1,2]. These states could be well reproduced by shell-model calculations in a valence space restricted to the *sd* shell using the USD residual interaction introduced by Brown and Wildenthal [3].

The *sd*-shell nuclei are presently the subject of renewed interest. Important aspects such as the occurrence of superdeformed shapes [4] associated with α clusterization [5] or the role of the isoscalar and isovectorial coupling at high-spin [6] have been theoretically investigated in recent years, pointing to more complex structures in these nuclei. Efforts have been also made to elucidate the residual interactions in large-scale shell-model calculations in the *sdfp* valence space [7]. On the experimental side, the use of heavy-ion beams in conjunction with large γ- and particle-detector arrays offers a powerful tool to study the level schemes of the *sd*-shell nuclei at high spins. Interesting results, pointing to a complex structure of coexisting spherical, deformed, and superdeformed states, were recently reported in ^{36}Ar [8,9] and ^{38}Ar [10].

A program to investigate the nuclei near ^{32}S using fusion-evaporation reactions and the γ- and particle-multidetector array GASP + ISIS has been undertaken at the Legnaro National Laboratory [11–15], with the aim to extend the level schemes at high spins for a comparison with detailed theoretical shell-model calculations. The present paper is devoted to the investigation of the high-spin level scheme of $^{31}_{15}$P$_{16}$. The experimental results are presented in Sec. II and are discussed in the framework of the shell model in Sec. III. Preliminary results have been previously reported in Ref. [11].

II. EXPERIMENTAL PROCEDURE AND RESULTS

The ^{31}P nucleus was populated via the ^{24}Mg(^{16}O,2αp) reaction with a 70-MeV ^{16}O beam delivered by the XTU Tandem Accelerator of the Legnaro National Laboratory. Two independent experiments were performed. In the first experiment, devoted to spectroscopic investigation, the target was a self-supporting ^{24}Mg foil with a thickness of 400 μg/cm^2. In the second experiment a target consisting of 750 μg/cm^2 ^{24}Mg, backed with 15 mg/cm^2 ^{197}Au, was employed for lifetime determinations by the Doppler shift attenuation method (DSAM). Coincident γ rays were detected with the GASP array comprising 40 Compton-suppressed HPGe detectors and an 80-element BGO ball, which acts as a

γ-ray multiplicity and sum filter [16]. Events were collected when at least two HPGe detectors and one BGO scintillator fired in coincidence. Energy and efficiency calibration were performed with standard sources of ^{56}Co and ^{152}Eu. In the thin-target experiment, for the purpose of channel selection and kinematical reconstruction the 4π charged-particle detector ISIS consisting of 40 ΔE-E Si telescopes [17] was also used.

The data from the thin-target measurement have been sorted into several γ-γ matrices in coincidence with the detection of two α particles and one proton. To improve the energy resolution, the recoil direction has been kinematically reconstructed. A symmetric γ-γ matrix, as well as three asymmetric matrices, having on the first axis the detectors in rings at 34°, 90°, and 146°, respectively, and on the second axis all the other detectors, have been created. The symmetric matrix has been used to study γ-γ coincidence relationships for the construction of the level scheme; the asymmetric matrices were used to obtain information about the γ transition multipolarities. For this purpose, the γ intensities corrected for efficiencies, from spectra gated on the axis with all the detectors, were used to calculate the ratio R_{ADO} defined as

$$R_{\mathrm{ADO}} = \frac{I_\gamma(34^\circ) + I_\gamma(146^\circ)}{2I_\gamma(90^\circ)}. \quad (1)$$

In the present experimental conditions, the angular distribution ratios have the values $R_{\mathrm{ADO}} \approx 0.8$ for pure dipole stretched transitions ($I \rightarrow I-1$), $R_{\mathrm{ADO}} \approx 1.35$ for quadrupole stretched transitions ($I \rightarrow I-2$), and $R_{\mathrm{ADO}} \approx 1.4$ for transitions with $\Delta I = 0$. In the case of mixed multipolarities, R_{ADO} depends on the value and sign of the mixing coefficient δ (see the following).

The data registered in the gold-backed target experiment were sorted to create a symmetric γ-γ matrix and seven asymmetric matrices having on the first axis the detectors in rings at 34°, 60°, 72°, 90°, 108°, 120°, and 146°, respectively, and on the second axis all the other detectors. The symmetric matrix has been used for the level scheme construction, whereas the asymmetric matrices have been used for lifetime determinations.

A. The level scheme of ^{31}P

States in ^{31}P have been investigated previously by β-decay, electron scattering, (p, γ), (α, γ), and transfer reactions [1,2]. The highest spin assigned in this nucleus was $I = 11/2$ for the 7441- and 6824-keV levels of positive and negative parity, respectively.

In the present work the level scheme was considerably extended at higher spins and excitation energies. Sixteen new states, eight of positive parity and eight of negative parity, have been observed at excitation energies >7.5 MeV and spins $I \geqslant 11/2$. The deduced level scheme of the ^{31}P nucleus, containing 64 new γ transitions, is shown in Fig. 1. The energy and intensity of the observed transitions, the R_{ADO} ratios, and the assigned multipolarities, as well as the energy and spin assignments for the corresponding states, are given in Table I.

The level scheme has been constructed on the basis of coincidence relationships in spectra created with appropriate gates on the symmetric γ-γ matrices from both thin and gold-backed target experiments. Figure 2 illustrates a spectrum obtained in the thin-target experiment with coincidence gates on the γ rays of 1266 and 2234 keV, which are depopulating the first two levels in ^{31}P. An interesting feature revealed in spectra from the experiment with the gold-backed target was that most γ rays assigned to ^{31}P present unshifted components. This is due to the peculiar fact that two states located at high excitation energy, namely the 10520- and 11297-keV states, have rather long lifetimes, of about 1 and 2 ps, respectively (see Sec. II B), and therefore their decay takes place mostly in stopped ^{31}P nuclei. Figure 3 illustrates a spectrum obtained in the gold-backed target experiment with coincidence gate on the 777-keV γ ray de-exciting the 11297-keV state. One notices the markedly better energy resolution as compared to that in the thin-target experiment (see Fig. 2), a fact that allowed a higher precision in the determination of the γ-ray energies and an increased sensitivity. Even for weakly populated states de-exciting transitions with branching ratios down to 1% could be observed. As shown in Fig. 1, a complex decay has been found for most of the new identified levels, with up to eight de-exciting transitions, as observed in the case of the 10217- and 10520-keV states.

Spins and parities for the new levels have been assigned on the basis of transition multipolarities deduced from measured R_{ADO} values and/or lifetime considerations. R_{ADO} values can be derived for the transitions with enough intensity. In Table I, these ratios are reported not only for new transitions but also for transitions whose multipolarities are known from previous studies [1]. The analysis of these data provided useful information for multipolarity assignments. Note that many previously known ($I \rightarrow I-1$) transitions have a $M1 + E2$ mixed character [1]. Comparison of the experimental R_{ADO} values with the calculated ones gives a hint as to the spin-dependent nuclear alignment. By assuming a Gaussian distribution of magnetic substates, a smooth decrease of the σ/I values with spin has been obtained, from $\sigma/I \approx 1.2$ at $I = 5/2$ to $\sigma/I \approx 0.7$ at highest spin. Using these data, on the basis of the measured R_{ADO} values it was possible to deduce multipolarities for 19 new γ transitions. All the new $I \rightarrow I-2$ quadrupole transitions included in the level scheme were assigned as $E2$, the $M2$ multipolarity being ruled out on the basis of measured lifetimes (see the following). Several $I \rightarrow I-1$ transitions were assigned as $M1 + E2$ mixed transitions, similar to previously known lower lying transitions [1]. For almost all the new states there is at least one transition with measured R_{ADO} and deduced multipolarity. The spin and parity assignment, based on these data, was further checked to be consistent with the multipolarities for all the other feeding and de-exciting transitions.

The yrast states $13/2^-$ at 8705 keV and $15/2^-$ at 10217 keV were identified based on the observation of the 1881-keV transition of $M1 + E2$ mixed character and of

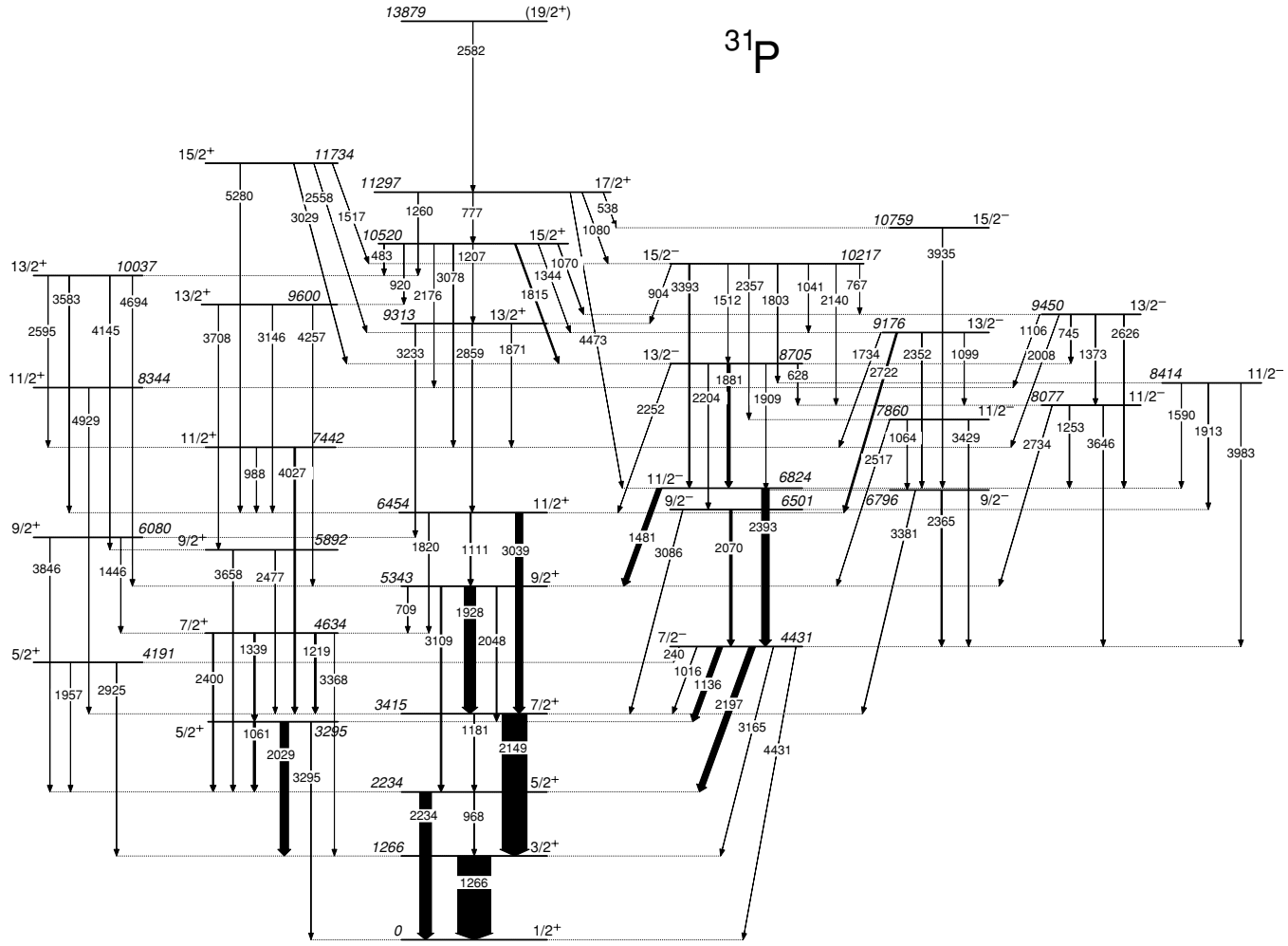

FIG. 1. Level scheme of ^{31}P deduced from the present work. The transitions between states of the same parity are shown as vertical arrows; the transitions connecting states of different parities are shown as tilted arrows.

the 3393-keV $E2$ transition, respectively, feeding the $11/2^-$ 6824-keV state. Three new $11/2^-$ states were found at 7860, 8077, and 8414 keV, de-exciting by $E2$ transitions to the $7/2^-$ 4431-keV state. The 9176-keV state assigned as the $13/2^-_2$ state is fed by the 1041-keV $M1 + E2$ transition from the $15/2^-_1$ state at 10217 keV. The assignment is supported by the pure dipole character of the 2722-keV de-exciting transition to the $11/2^+$ 6454-keV state. The spin-parity assignment for the $13/2^-_3$ state at 9450 keV was based on the measured R_{ADO} values for the 745-keV $\Delta I = 0$ transition to the $13/2^-_1$ state and the 2626-keV $M1 + E2$ transition to the $11/2^-_1$ state. The level at 10759 keV decaying by the 3935-keV $E2$ transition to the $11/2^-$ yrast state was assigned as the $15/2^-_2$ state. On the positive-parity side the yrast $13/2^+$ state has been identified at 9313 keV excitation energy based on the observation of the 2859-keV transition of $M1 + E2$ mixed character, feeding the $11/2^+$ 6454-keV state. The $11/2^+_3$ state at 8344 keV and the two yrare $13/2^+$ states at 9600 and 10037 keV are de-excited by $E2$ transitions to the yrast $7/2^+$ and $9/2^+$ states, respectively. A spin of 15/2 was assigned to the 10520-keV state as it decays via the 1815-keV transition of pure dipole character to the $13/2^-_1$ state, whereas for the 11297-keV state a spin 17/2 was assigned based on the $M1 + E2$ mixed character of the 777-keV transition feeding the 15/2 state. The positive parity for these two states was established on the basis of the 1260-keV $E2$ transition from the 17/2 state to the $13/2^+_3$ state. This assignment was also supported by the observation of a weak branch of 4473 keV linking the $17/2^+$11297-keV and $11/2^-$ 6824-keV states, assigned as an $E3$ transition, a $M3$ multipolarity being ruled out by the measured lifetime. The 11734-keV state de-excited by the 5280-keV $E2$ transition to the $11/2^+$ 6454-keV state was assigned as the $15/2^+_2$ state. R_{ADO} could not be measured for the weak 2582-keV transition de-exciting the 13879-keV level, and therefore the spin-parity assignment of $(19/2^+)$ for this state is only tentative.

As seen in Fig. 1, the positive-parity and negative-parity states in the level scheme form two almost independent structures. They are connected by $E1$ transitions from the negative-parity to the positive-parity states, identified at

TABLE I. Transition energies and relative intensities of the γ rays, angular distribution ratios, multipolarities and mixing coefficients, and the energy and spin assignment for the initial and final states in ^{31}P.

E_γ(keV)	$I_\gamma^{\rm rel}$	$R_{\rm ADO}$	Mult.	δ	E_i(keV)	E_f(keV)	I_i^π	I_f^π
239.8(2)	2.6(5)				4431	4191	$7/2_1^-$	$5/2_3^+$
483.1(2)	2.1(5)				10520	10037	$15/2_1^+$	$13/2_3^+$
537.5(2)	1.9(4)				11297	10759	$17/2_1^+$	$15/2_2^-$
628.4(2)	4.8(4)				8705	8077	$13/2_1^-$	$11/2_3^-$
709.4(2)	5.4(8)				5343	4634	$9/2_1^+$	$7/2_2^+$
744.7(2)	14(2)	1.44(16)	$M1$		9450	8705	$13/2_3^-$	$13/2_1^-$
767.3(2)	3.1(6)				10217	9450	$15/2_1^-$	$13/2_3^-$
776.8(2)	15(2)	1.04(10)	$M1+E2$	+0.17(10)	11297	10520	$17/2_1^+$	$15/2_1^+$
903.9(3)	2.2(4)				10217	9313	$15/2_1^-$	$13/2_1^+$
920.4(3)	3.2(7)				10520	9600	$15/2_1^+$	$13/2_2^+$
967.6(3)	7.1(5)				2234	1266	$5/2_1^+$	$3/2_1^+$
988.4(2)	10(1)	1.63(35)	$M1+E2$	+0.6(3)[a]	7442	6454	$11/2_2^+$	$11/2_1^+$
1016.4(2)	16(2)	1.43(21)	$E1$		4431	3415	$7/2_1^-$	$7/2_1^+$
1041.0(2)	10(2)	1.47(22)	$M1+E2$	$\geqslant$+0.30	10217	9176	$15/2_1^-$	$13/2_2^-$
1061.0(3)	73(3)	1.32(7)	$M1+E2$	+0.40(5)[a]	3295	2234	$5/2_2^+$	$5/2_1^+$
1063.5(4)	14(1)				7860	6796	$11/2_2^-$	$9/2_2^-$
1069.8(3)	18(2)				10520	9450	$15/2_1^+$	$13/2_3^-$
1080.1(3)	8(2)				11297	10217	$17/2_1^+$	$15/2_1^-$
1099.2(4)	8(3)				9176	8077	$13/2_2^-$	$11/2_3^-$
1106.4(4)	1.0(4)				9450	8344	$13/2_3^-$	$11/2_3^+$
1110.5(3)	38(4)	1.13(10)	$M1+E2$	+0.27(3)[a]	6454	5343	$11/2_1^+$	$9/2_1^+$
1135.7(3)	161(9)	0.83(4)	$E1$		4431	3295	$7/2_1^-$	$5/2_2^+$
1181.1(3)	24(2)	0.48(9)	$M1+E2$	−0.35(7)[a]	3415	2234	$7/2_1^+$	$5/2_1^+$
1207.3(4)	2.5(8)				10520	9313	$15/2_1^+$	$13/2_1^+$
1218.8(3)	50(2)	1.44(9)	$M1+E2$	+0.33(6)[a]	4634	3415	$7/2_2^+$	$7/2_1^+$
1253.4(3)	22(2)	1.25(15)	$M1$		8077	6824	$11/2_3^-$	$11/2_1^-$
1259.6(4)	6.0(7)				11297	10037	$17/2_1^+$	$13/2_3^+$
1266.1(4)	1000(28)	0.75(2)	$M1+E2$	−0.30(1)[a]	1266	0	$3/2_1^+$	$1/2_1^+$
1338.7(4)	48(4)	1.15(10)	$M1+E2$	+0.38(4)[a]	4634	3295	$7/2_2^+$	$5/2_2^+$
1344.3(5)	0.9(3)				10520	9176	$15/2_1^+$	$13/2_2^-$
1373.2(5)	8(1)				9450	8077	$13/2_3^-$	$11/2_3^-$
1445.6(4)	12(2)	0.94(13)	$M1+E2$	+0.13(8)	6080	4634	$9/2_3^+$	$7/2_2^+$
1480.8(3)	151(6)	0.81(4)	$E1$		6824	5343	$11/2_1^-$	$9/2_1^+$
1511.9(5)	1.6(4)				10217	8705	$15/2_1^-$	$13/2_1^-$
1516.8(5)	16(3)	1.31(18)	$E1$		11734	10217	$15/2_2^+$	$15/2_1^-$
1590.1(5)	11(2)	1.37(11)	$M1$		8414	6824	$11/2_4^-$	$11/2_1^-$
1733.9(6)	9(3)				9176	7442	$13/2_2^-$	$11/2_2^+$
1802.8(5)	6(1)				10217	8414	$15/2_1^-$	$11/2_4^-$
1814.5(4)	42(4)	0.81(8)	$E1$		10520	8705	$15/2_1^+$	$13/2_1^-$
1819.6(6)	6.1(6)				6454	4634	$11/2_1^+$	$7/2_2^+$
1871.1(6)	12(6)				9313	7442	$13/2_1^+$	$11/2_2^+$
1881.3(4)	95(8)	1.08(7)	$M1+E2$	+0.20(6)	8705	6824	$13/2_1^-$	$11/2_1^-$
1909.2(5)	9(1)				8705	6796	$13/2_1^-$	$9/2_2^-$
1913.1(5)	7(3)				8414	6501	$11/2_4^-$	$9/2_1^-$
1928.4(4)	337(13)	0.82(4)	$M1+E2$	+0.04(6)[a]	5343	3415	$9/2_1^+$	$7/2_1^+$
1957.2(6)	5.5(6)				4191	2234	$5/2_3^+$	$5/2_1^+$
2007.8(7)	2(1)				9450	7442	$13/2_3^-$	$11/2_2^+$
2028.6(4)	259(9)	1.16(4)	$M1+E2$	+0.40(2)[a]	3295	1266	$5/2_2^+$	$3/2_1^+$
2048.3(4)	29(4)	1.32(12)	$E2$		5343	3295	$9/2_1^+$	$5/2_2^+$
2070.4(4)	71(4)	1.72(20)	$M1+E2$	+1.3(3)[a]	6501	4431	$9/2_1^-$	$7/2_1^-$
2139.6(5)	5.4(8)				10217	8077	$15/2_1^-$	$11/2_3^-$
2148.6(4)	754(26)	1.44(4)	$E2$		3415	1266	$7/2_1^+$	$3/2_1^+$
2176.4(6)	0.9(2)				10520	8344	$15/2_1^+$	$11/2_3^+$
2197.0(4)	186(6)	0.83(5)	$E1$		4431	2234	$7/2_1^-$	$5/2_1^+$
2203.6(6)	9(2)				8705	6501	$13/2_1^-$	$9/2_1^-$
2233.5(4)	259(44)	1.24(8)	$E2$		2234	0	$5/2_1^+$	$1/2_1^+$

TABLE I. (*Continued*.)

E_γ(keV)	$I_\gamma^{\rm rel}$	$R_{\rm ADO}$	Mult.	δ	E_i(keV)	E_f(keV)	I_i^π	I_f^π
2251.6(5)	8(1)				8705	6454	$13/2_1^-$	$11/2_1^+$
2351.6(6)	5(1)				9176	6824	$13/2_2^-$	$11/2_1^-$
2356.8(6)	8(2)				10217	7860	$15/2_1^-$	$11/2_2^-$
2365.0(4)	42(3)	0.70(5)	$M1+E2$	$-0.29(4)$[a]	6796	4431	$9/2_2^-$	$7/2_1^-$
2393.0(4)	229(6)	1.47(7)	$E2$		6824	4431	$11/2_1^-$	$7/2_1^-$
2399.7(5)	34(4)				4634	2234	$7/2_2^+$	$5/2_1^+$
2477.3(6)	2.3(7)				5892	3415	$9/2_2^+$	$7/2_1^+$
2516.8(6)	10(1)	0.85(11)	$E1$		7860	5343	$11/2_2^-$	$9/2_1^+$
2557.7(9)	8(2)				11734	9176	$15/2_2^+$	$13/2_2^-$
2582.1(9)	7(3)				13879	11297	$19/2_1^+$	$17/2_1^+$
2594.7(6)	4(2)				10037	7442	$13/2_3^+$	$11/2_2^+$
2625.7(6)	14(1)	1.31(21)	$M1+E2$	$\geqslant+0.2$	9450	6824	$13/2_3^-$	$11/2_1^-$
2722.3(5)	50(4)	0.84(7)	$E1$		9176	6454	$13/2_2^-$	$11/2_1^+$
2733.6(6)	11(2)				8077	5343	$11/2_3^-$	$9/2_1^+$
2859.1(6)	18(2)	1.16(18)	$M1+E2$	$+0.25(10)$	9313	6454	$13/2_1^+$	$11/2_1^+$
2924.7(6)	15(1)				4191	1266	$5/2_3^+$	$3/2_1^+$
3028.5(9)	14(3)				11734	8705	$15/2_2^+$	$13/2_1^-$
3038.7(5)	225(7)	1.24(7)	$E2$		6454	3415	$11/2_1^+$	$7/2_1^+$
3078.1(6)	1.8(3)				10520	7442	$15/2_1^+$	$11/2_2^+$
3086.4(6)	13(1)				6501	3415	$9/2_1^-$	$7/2_1^+$
3109.4(6)	47(3)	1.27(16)	$E2$		5343	2234	$9/2_1^+$	$5/2_1^+$
3145.7(7)	0.9(4)				9600	6454	$13/2_2^+$	$11/2_1^+$
3164.6(7)	9(2)				4431	1266	$7/2_1^-$	$3/2_1^+$
3233.4(7)	5(1)				9313	6080	$13/2_1^+$	$9/2_3^+$
3294.7(7)	2.8(5)				3295	0	$5/2_2^+$	$1/2_1^+$
3367.6(7)	5(2)				4634	1266	$7/2_2^+$	$3/2_1^+$
3380.7(6)	16(3)				6796	3415	$9/2_2^-$	$7/2_1^+$
3392.5(6)	40(9)	1.34(14)	$E2$		10217	6824	$15/2_1^-$	$11/2_1^-$
3428.6(6)	20(1)	1.36(17)	$E2$		7860	4431	$11/2_2^-$	$7/2_1^-$
3582.8(7)	1.3(5)				10037	6454	$13/2_3^+$	$11/2_1^+$
3645.6(7)	9(2)	1.28(31)	$E2$		8077	4431	$11/2_3^-$	$7/2_1^-$
3658.2(5)	24(2)	1.31(21)	$E2$		5892	2234	$9/2_2^+$	$5/2_1^+$
3707.6(7)	2(1)				9600	5892	$13/2_2^+$	$9/2_2^+$
3846.3(7)	24(2)				6080	2234	$9/2_3^+$	$5/2_1^+$
3934.6(7)	15(2)	1.27(25)	$E2$		10759	6824	$15/2_2^-$	$11/2_1^-$
3983.3(7)	9(1)	1.35(21)	$E2$		8414	4431	$11/2_4^-$	$7/2_1^-$
4026.6(5)	53(2)	1.37(13)	$E2$		7442	3415	$11/2_2^+$	$7/2_1^+$
4144.5(7)	1.7(5)				10037	5892	$13/2_3^+$	$9/2_2^+$
4257.1(8)	0.6(3)				9600	5343	$13/2_2^+$	$9/2_1^+$
4431.0(7)	2.8(6)				4431	0	$7/2_1^-$	$1/2_1^+$
4472.7(9)	0.6(2)				11297	6824	$17/2_1^+$	$11/2_1^-$
4693.6(8)	10(2)	1.36(28)	$E2$		10037	5343	$13/2_3^+$	$9/2_1^+$
4928.5(8)	11(1)	1.38(29)	$E2$		8344	3415	$11/2_3^+$	$7/2_1^+$
5280.3(19)	7(1)	1.51(31)	$E2$		11734	6454	$15/2_2^+$	$11/2_1^+$

[a]From Ref. [1].

both low and high spins. All positive-parity states with $I \leqslant 13/2^+$ decay only to states of the same parity. An interesting feature of the decay scheme is the clear change in the de-excitation of the positive-parity states with $I^\pi > 13/2^+$. In contrast to the lower spin states, the $15/2^+$ and $17/2^+$ states decay significantly to the negative-parity states. This behavior indicates a change of structure at the high-spin states that could involve nucleon excitations in the negative-parity orbitals.

B. Lifetime measurements

In previous studies lifetimes for the low-spin states in ^{31}P have been reported [1]. The longest lifetimes, $\tau = 0.745(35)$ and 0.6(1) ps, were measured for the $3/2^+$ 1266-keV and $7/2^-$ 4431-keV states, respectively. For the other states shorter lifetimes, down to several femtoseconds, have been determined.

In the present work the lifetimes of the new high-spin states have been investigated by the DSAM. From the asymmetric

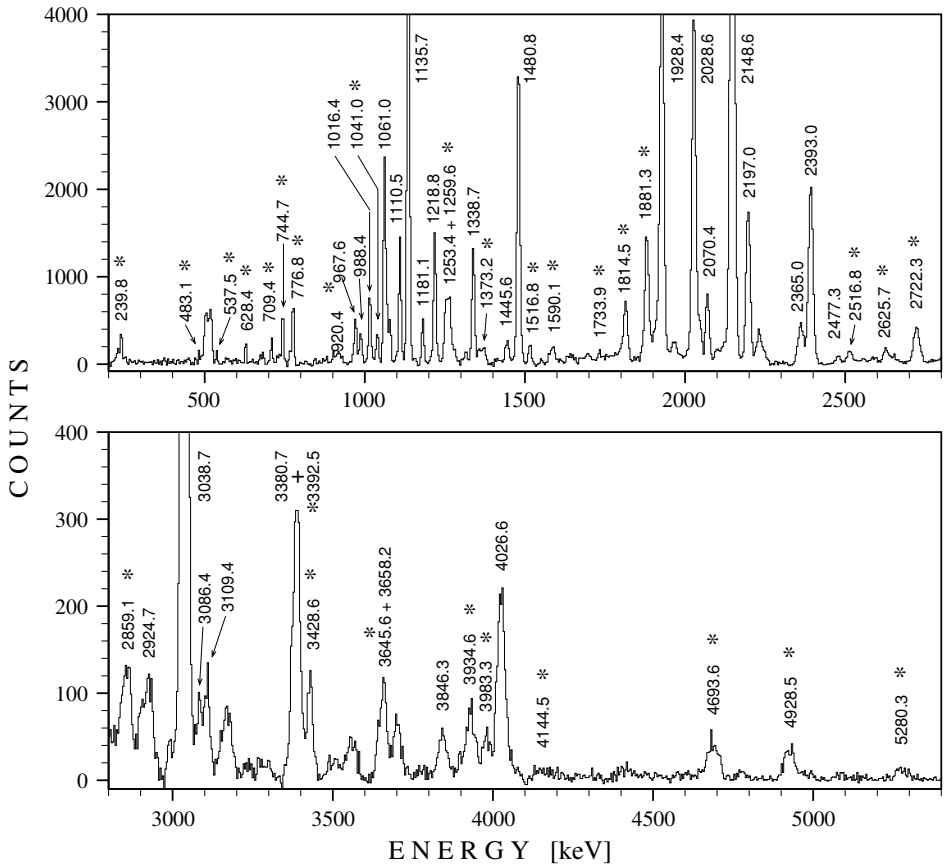

FIG. 2. Coincidence spectrum with gates on the 1266.1- and 2233.5-keV γ rays from the thin-target measurement. The γ rays in ^{31}P are labeled with their energy. The new assigned γ rays are marked with a star.

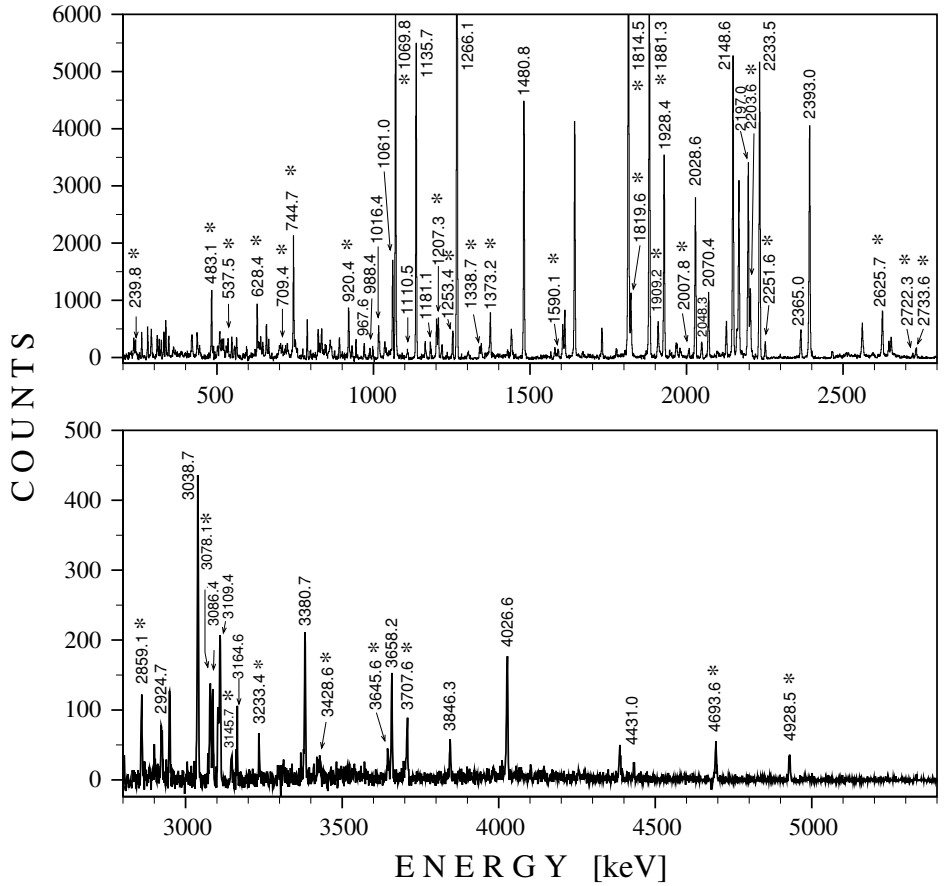

FIG. 3. Coincidence spectrum with gate on the 777-keV γ ray from the thick-target measurement. The γ rays in ^{31}P are labeled with their energy. The new assigned γ rays are marked with a star.

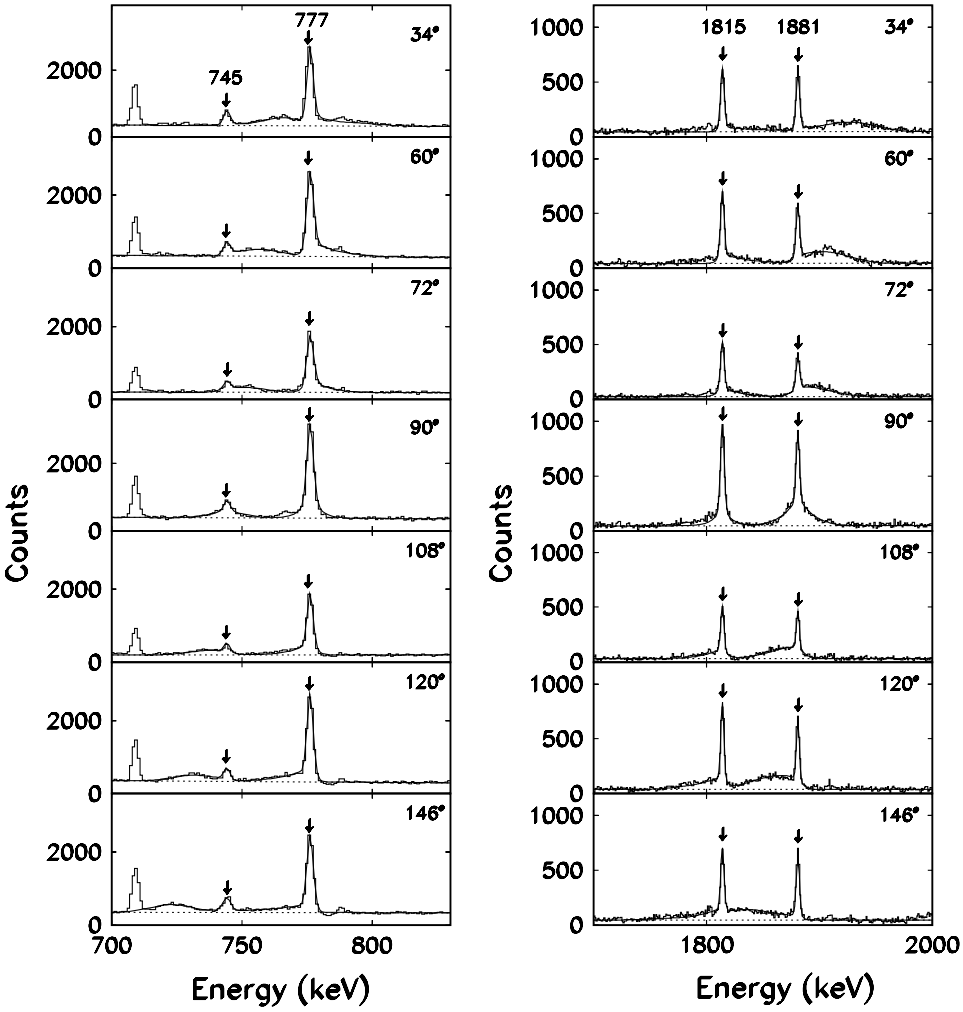

FIG. 4. Experimental and calculated line shapes for the 745-, 777-, 1815-, and 1881-keV transitions de-exciting the states at 11297, 9450, 10520, and 8705 keV, respectively, in ^{31}P.

matrices obtained in the gold-backed target experiment, spectra have been created with narrow gates on the low-lying transitions emitted from stopped nuclei. The analysis has been performed using the LINESHAPE computer code [18] modified to allow, at each level, side populations from independent levels. This was particularly important in the present case where most levels have a fraction of their population coming from longer lived states. The slowing down history of ^{31}P recoils in the target and backing was simulated using Monte Carlo techniques and a statistical distribution was created for the projection of the recoil velocity with respect to the direction of the detected γ ray. The shell-corrected Northcliffe and Schilling stopping powers [19] were used. Examples of experimental line shapes at different angles and the corresponding fits are illustrated in Fig. 4. Lifetimes could be extracted for six new levels, four of negative parity and two of positive parity, as shown in Table II. The other new high-spin states investigated in the present work are rather weakly populated, a fact that prevented a precise lifetime analysis. However, very short lifetimes (<50 fs) are indicated for them on the basis of the observed shifted peaks at various angles. The lifetime information obtained for the new high-spins states in ^{31}P gives support to the $E2$ multipolarity assignment for the quadrupole transitions involved in their decay, as the $M2$ multipolarity would correspond to transition strengths much higher than the upper limit of 3 W.u. recommended for this mass region [20].

As seen in Table II, contrary to the usual trend of decreasing lifetimes with increasing spins, rather long lifetimes have been derived for the 11297-keV $17/2^+$ and 10520-keV $15/2^+$ states. This is another characteristic pointing to a different structure of these high-spin positive-parity states.

TABLE II. Lifetimes determined in the present work for high-spin states in ^{31}P.

E_x (keV)	I^π	τ (ps)
8705	$13/2_1^-$	0.23(4)
9176	$13/2_2^-$	0.12(4)
9450	$13/2_3^-$	0.05(2)
10217	$15/2_1^-$	0.11(3)
10520	$15/2_1^+$	0.97(10)
11297	$17/2_1^+$	1.9(2)

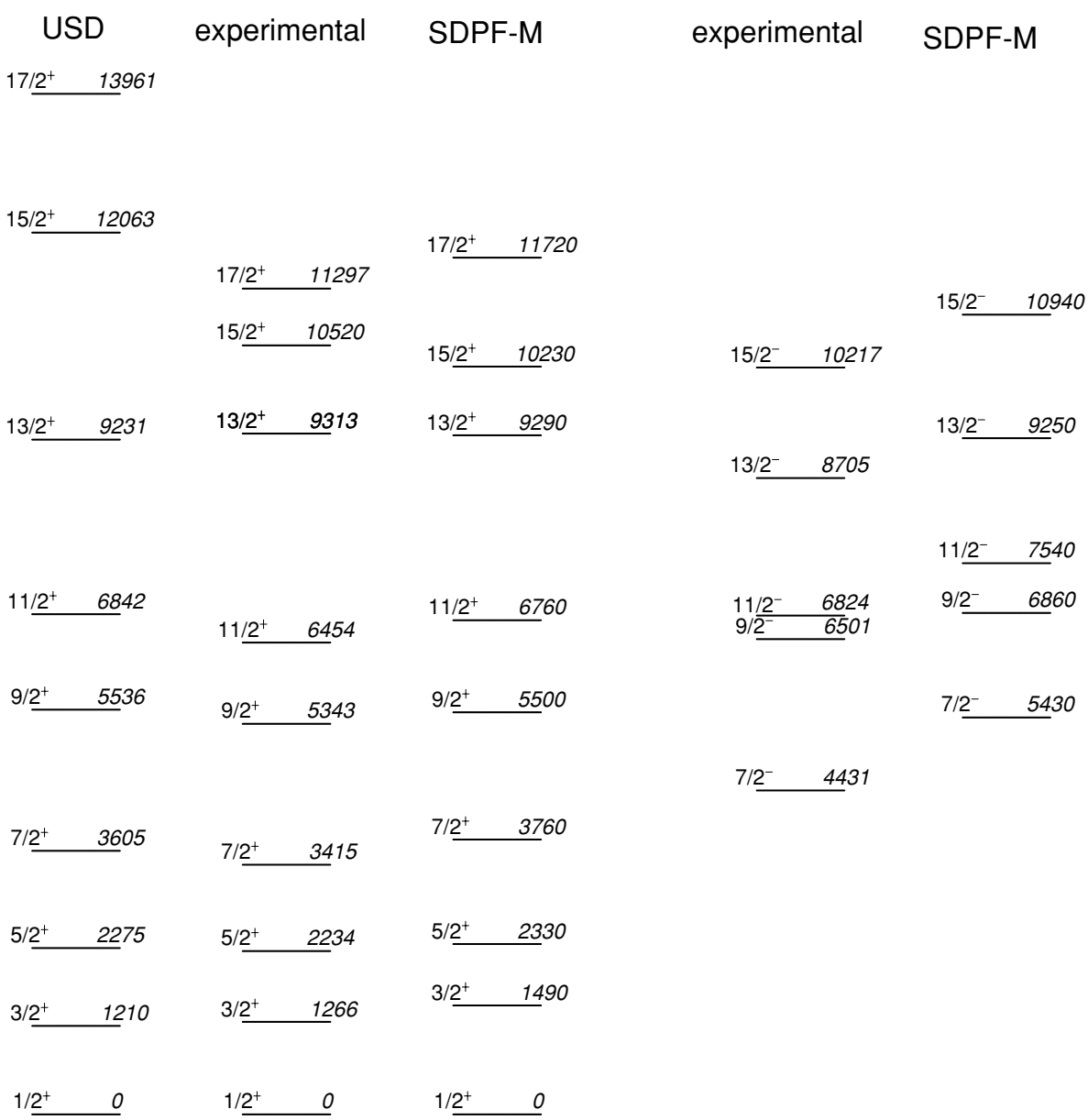

FIG. 5. Experimental yrast levels of ^{31}P compared to shell-model calculations (see text for details).

III. DISCUSSION

To interpret the observed properties in ^{31}P, detailed shell-model calculations for both excitation energies and γ transition probabilities have been performed. A first calculation (*sd*) was performed with the code ANTOINE [21] in the *sd* shell-model space using the USD residual interaction [3]. The comparison between the experimental yrast positive-parity levels and the calculated ones is illustrated on the left side of Fig. 5. We note the remarkable agreement between experimental and calculated states up to spin $13/2^+$. However, the $15/2^+$ and $17/2^+$ yrast states are predicted too high in energy. This indicates that at high spins the *sd* shell-model space is not enough for a good description of the states and that intruder excitations into the *fp* shell have to be considered.

To better reproduce the positive-parity high-spin states and to describe the negative-parity states, a second calculation has been performed with the Monte Carlo shell model (MCSM) [22]. The valence space in this case was $d_{5/2}s_{1/2}d_{3/2}f_{7/2}p_{3/2}$ and the interaction consisted of three parts. The USD [3] and the Kuo-Brown [23] interactions have been used for the *sd* and *fp* shell, respectively, whereas for the cross-shell part, the interaction of Ref. [24], based on the Millener-Kurath interaction [25], has been adopted. To correct the neutron dripline of oxygen isotopes small but rather important corrections have been made to the USD part. This combined interaction has been introduced in Ref. [7]; it was named as

TABLE III. Experimental level energies in ^{31}P (from Ref. [1] and present work) compared with calculated values using the Monte Carlo shell model and the SDPF-M interaction. For each state are given the occupation numbers in the *fp* shell for protons ($\pi\ fp$) and for neutrons ($\nu\ fp$).

I^π	$E_x^{\rm exp}$ (MeV)	$E_x^{\rm calc}$ (MeV)	$\pi\ fp$	νfp
$1/2^+$	0.00	0.00	0.06	0.11
	3.13	3.85	0.05	0.07
	5.01	5.59	0.05	0.07
$3/2^+$	1.27	1.49	0.07	0.12
	3.51	3.62	0.08	0.13
	4.26	5.28	0.04	0.06
$5/2^+$	2.23	2.33	0.07	0.11
	3.30	3.55	0.07	0.10
	4.19	4.42	0.08	0.11
$7/2^+$	3.42	3.76	0.07	0.11
	4.63	5.16	0.07	0.09
	5.53	5.80	0.07	0.09
$9/2^+$	5.34	5.50	0.07	0.11
	5.89	5.92	0.06	0.10
	6.08	6.36	0.08	0.10
$11/2^+$	6.45	6.76	0.07	0.10
	7.44	7.72	0.06	0.09
	8.34	8.61	0.06	0.09
$13/2^+$	9.31	9.29	0.07	0.09
	9.60	10.71	0.09	0.11
	10.04	10.90	0.06	0.09
$15/2^+$	10.52	10.23	1.00	1.02
	11.73	12.22	0.08	0.11
$17/2^+$	11.30	11.72	1.01	1.02
$7/2^-$	4.43	5.43	0.66	0.50
$9/2^-$	6.50	6.86	0.12	0.94
	6.80	7.19	0.32	0.82
$11/2^-$	6.83	7.54	0.51	0.57
	7.86	8.18	0.23	0.85
	8.08	8.74	0.21	0.89
$13/2^-$	8.71	9.25	0.20	0.87
	9.18	9.85	0.24	0.85
	9.45	10.09	0.13	0.94
$15/2^-$	10.22	10.94	0.40	0.68
	10.76	11.62	0.14	0.92

the SDPF-M interaction in Ref. [26]. One can find in Ref. [7] how the SDPF-M interaction is constructed from the known pieces of interactions and additional improvement.

The calculated level energies are compared with the experimental ones in Fig. 5 and Table III. As seen in Fig. 5, the positive-parity yrast states are well described by the MCSM calculations, up to the highest spin state $17/2^+$. To see the contribution of the intruder proton and neutron excitations, their occupation numbers in the $f_{7/2}p_{3/2}$ orbits are also given in Table III. The contribution of nucleon excitation to the *fp* shell is very small for $I^\pi \leqslant 13/2^+$, in agreement with *sd* calculations, but becomes important for the $I^\pi = 15/2^+$ and $17/2^+$ states. Note that the decay properties of these two states, which are significantly populating the negative-parity states, give support to this description. In fact, being the electromagnetic operator one-body, the de-excitation of states with two particles in the *fp* shell proceeds via the negative-parity states with one intruder excitation. The promotion to the *fp* shell of a proton-neutron pair, coupled to $T = 0$, is energetically favored with respect to the promotion of a pair of protons or neutrons with $T = 1$. This type of coupling has been observed also in the high spin structure of ^{34}S [15].

Negative-parity states are also rather well described by the MCSM calculations (see right side of Fig. 5 and the lower part of Table III). An overestimation of about 600 keV is observed for the calculated states. This could indicate that the $d_{3/2}$-$f_{7/2}$ gap produced by the SDPF-M interaction, which is about 5.3 MeV for P isotopes with $N \sim 20$, may be too large. Although it is thus likely that the gap is smaller than 5.3 MeV for P isotopes, we need further studies to pin down the gap size more precisely. An interesting feature revealed by the calculations is that the yrast negative-parity states show an alternating structure: the $7/2^-$, $11/2^-$, and $15/2^-$ states are described by almost equal contributions of the proton and neutron excitation to the *fp* shell, whereas the $9/2^-$ and $13/2^-$ states have only a neutron excitation to the $f_{7/2}$ shell. This behavior is in accordance with the simple picture describing the states in ^{31}P by coupling one nucleon to the states from neighboring nuclei. Thus the $7/2^-$, $11/2^-$, and $15/2^-$ states could arise from the coupling of the 0^+, 2^+, and 4^+ states in ^{30}Si and ^{30}P with a proton and a neutron in the $f_{7/2}$ orbit, respectively. However, the $9/2^-$ and $13/2^-$ states, with configurations dominated by $\pi(s_{1/2})\ \nu(s_{1/2}f_{7/2})$ and $\pi(d_{3/2})\ \nu(d_{3/2}f_{7/2})$, respectively, arise by coupling one neutron in the $f_{7/2}$ shell to the low-lying 1^+ and 3^+ states in ^{30}P.

Using the measured lifetimes τ (from Ref. [1] and this work) and the branching ratios (*BR*) derived from the presently determined γ-ray intensities, the experimental reduced transition probabilities have been obtained. For $M1 + E2$ mixed transitions the mixing coefficients δ from Table I were used to estimate the corresponding partial lifetimes.

The experimental $B(M1)$ and $B(E2)$ values are compared in Tables IV and V with shell-model calculations for positive- and negative-parity states, respectively. In the case of low- and medium-spin positive-parity states the transition strengths were derived using both the ANTOINE code with the USD interaction and the MCSM with the SDPF-M interaction. For the $15/2^+$ and $17/2^+$ high-spin states involving a larger contribution of nucleon excitation to the *fp* shell, as well as for the negative-parity states, the calculations were done with the MCSM approach and the SDPF-M interaction.

The predictions of the *sd* and MCSM calculations are similar and in an overall good agreement with experimental $B(M1)$ and $B(E2)$ values for transitions from low- and medium-spin positive-parity states (see Table IV). In view of the high sensitivity of the transition probabilities to the composition of the wave function, this agreement is quite remarkable. With few exceptions, the observed $B(M1)$ and $B(E2)$ are well reproduced by the MCSM calculations also for the negative-parity states (see Table V). This gives further support for the validity of the SDPF-M effective interaction [7] used in these calculations.

TABLE IV. Experimental reduced transition probabilities $B(M1)$ and $B(E2)$ for positive-parity states in ^{31}P, compared to shell-model calculations performed with the code ANTOINE in the *sd* space using the USD residual interaction and with the Monte Carlo shell model and the SDPF-M interaction. In deriving the theoretical $B(M1)$ values free-nucleon g factors have been used. The theoretical $B(E2)$ values have been obtained using for the effective electric charges (e_ν, e_π) values of $(0.5e,1.5e)$ in the *sd* calculations and $(0.5e,1.3e)$ in the Monte Carlo shell-model calculations.

E_x (keV)	τ (fs)	I_i^π	I_f^π	E_γ (keV)	BR (%)	$B(M1)(\mu_N^2)$			$B(E2)\,(e^2\,\mathrm{fm}^4)$		
						Exp	USD	SDPF-M	Exp	USD	SDPF-M
1266	745(35)[a]	$3/2_1^+$	$1/2_1^+$	1266	100	0.034(2)	0.016	0.020	28(3)	38	37
2234	370(12)[a]	$5/2_1^+$	$3/2_1^+$	968	3(1)	0.005(2)	0.0003	0.003			
			$1/2_1^+$	2234	97(1)				39(3)	45	47
3295	115(20)[a]	$5/2_2^+$	$5/2_1^+$	1061	22(3)	0.08(2)	0.10	0.016	159(49)	63	52
			$3/2_1^+$	2029	77(4)	0.039(8)	0.063	0.031	22(5)	19	25
			$1/2_1^+$	3295	1.0(3)				0.18(5)	0.21	3.2
3415	315(40)[a]	$7/2_1^+$	$5/2_1^+$	1181	3.0(5)	0.003(1)	0.0001	0.001	4(2)	13	15
			$3/2_1^+$	2149	97(6)				54(8)	64	65
4191	7(3)[a]	$5/2_3^+$	$5/2_1^+$	1957	27(5)	0.29(13)	0.37	0.31			
			$3/2_1^+$	2925	73(7)	0.24(11)	0.34	0.32			
4634	110(15)[a]	$7/2_2^+$	$7/2_1^+$	1219	36(2)	0.09(2)	0.14	0.16	99(35)	20	13
			$5/2_2^+$	1339	35(2)	0.07(2)	0.05	0.04	78(18)	74	66
			$5/2_1^+$	2400	25(3)	0.008(2)	0.0007	0.003	4(1)	0.7	0.6
			$3/2_1^+$	3368	4(1)				0.7(2)	0.01	1.4
5343	60(15)[a]	$9/2_1^+$	$7/2_2^+$	709	2.0(5)	0.05(3)	0.01	0.01			
			$7/2_1^+$	1928	80(4)	0.10(3)	0.06	0.10			
			$5/2_2^+$	2048	7(1)				26(12)	19	20
			$5/2_1^+$	3109	11(1)				5(2)	20	18
5892	33(8)[a]	$9/2_2^+$	$7/2_1^+$	2477	9(3)	0.010(3)	0.012	0.024			
			$5/2_1^+$	3658	91(9)				34(10)	13	23
6080	32(15)[a]	$9/2_3^+$	$7/2_2^+$	1446	33(5)	0.20(10)	0.23	0.21			
			$5/2_1^+$	3846	67(8)				21(12)	25	22
6454	33(12)[a]	$11/2_1^+$	$9/2_1^+$	1111	14(2)	0.18(7)	0.01	0.01			
			$7/2_2^+$	1820	3(1)				37(17)	20	14
			$7/2_1^+$	3039	83(3)				79(31)	42	49
10520	970(100)[b]	$15/2_1^+$	$13/2_3^+$	483	3(1)	0.015(6)		<0.001			
			$13/2_2^+$	920	5(1)	0.036(8)		<0.001			
			$13/2_1^+$	1207	4(1)	0.001(1)		<0.001			
			$11/2_3^+$	2176	1.0(5)				0.21(11)		<0.1
			$11/2_2^+$	3078	3(1)				0.08(4)		<0.1
			$11/2_1^+$	4066	<1				<0.01		<0.1
11297	1900(200)[b]	$17/2_1^+$	$15/2_1^+$	777	48(9)	0.03(1)		0.482			
			$13/2_3^+$	1260	19(3)				26(5)		<0.1
			$13/2_2^+$	1697	<1				<0.30		<0.1
			$13/2_1^+$	1984	<1				<0.14		<0.1

[a]Reference [1].
[b]Present work.

The transition probabilities for the decay of the $15/2_1^+$ state to the $13/2^+$ and $11/2^+$ states are very small. This is in agreement with shell-model calculations, because the predicted configuration of the $15/2_1^+$ state involves the excitation of two particles to the *fp* shell, whereas the configuration of the lower positive-parity states involves mainly the *sd* shell. The same behavior would be expected for the decay of the $17/2_1^+$ state to the $13/2^+$ states. This is in agreement for the transitions to the first two $13/2^+$ states, whereas the transition to the $13/2_3^+$ state shows a non-negligible, although small, $B(E2)$. In contrast, the measured $B(M1)$ for the transition to the $15/2_1^+$ state is much smaller than the calculated $B(M1)$. These deviations may reflect a more complex structure of high-spin states in ^{31}P, which needs a more refined interaction and a wider model space in the shell-model calculation.

Monte Carlo shell-model calculations were performed to derive reduced transition probabilities for parity-changing $E1$ transitions in ^{31}P. The theoretical $B(E1)$ values are compared in Table VI with the experimental values. A satisfactory agreement is obtained for many cases. The most significant discrepancy between experimental and theoretical $B(E1)$ values is observed for the transitions de-exciting the $17/2_1^+$ state. For this state also the $M1$ and $E2$ de-exciting transitions were not satisfactory described, as already shown.

TABLE V. Experimental reduced transition probabilities $B(M1)$ and $B(E2)$ for negative-parity states in ^{31}P, compared to MCSM calculations performed using the SDPF-M interaction. In deriving the theoretical $B(M1)$ values free-nucleon g factors have been used. The theoretical $B(E2)$ values have been obtained using effective electric charges of $0.5e$ and $1.3e$ for the neutron and proton, respectively.

E_x (keV)	τ (fs)	I_i^π	I_f^π	E_γ (keV)	BR (%)	$B(M1)(\mu_N^2)$		$B(E2)(e^2\,\mathrm{fm}^4)$	
						Exp	SDPF-M	Exp	SDPF-M
6501	55(17)[a]	$9/2_1^-$	$7/2_1^-$	2070	85(7)	0.037(16)	0.046	207(77)	13
6796	202(42)[a]	$9/2_2^-$	$7/2_1^-$	2365	72(7)	0.014(4)	0.020	3(1)	58
6824	123(51)[a]	$11/2_1^-$	$7/2_1^-$	2393	60(3)			50(21)	20
8705	230(40)[b]	$13/2_1^-$	$11/2_3^-$	628	4(1)	0.039(11)	0.079		
			$11/2_1^-$	1881	76(8)	0.027(5)	0.001		
			$9/2_2^-$	1909	7(2)			10(3)	26
			$9/2_1^-$	2204	7(2)			5(2)	1.4
9176	120(40)[b]	$13/2_2^-$	$11/2_3^-$	1099	11(4)	0.038(16)	0.001		
			$11/2_1^-$	2352	11(3)	0.004(1)	0.009		
9450	50(20)[b]	$13/2_3^-$	$13/2_1^-$	745	36(7)	0.976(53)	0.073		
			$11/2_3^-$	1373	20(4)	0.091(49)	0.115		
			$11/2_1^-$	2626	36(4)	0.023(12)	0.016		
10217	110(30)[b]	$15/2_1^-$	$13/2_3^-$	767	4(1)	0.048(18)	0.093		
			$13/2_2^-$	1041	13(4)	0.059(24)	0.031		
			$13/2_1^-$	1512	2(1)	0.003(3)	0.007		
			$11/2_4^-$	1803	8(2)			30(12)	
			$11/2_3^-$	2140	7(2)			12(5)	12
			$11/2_2^-$	2357	10(3)			11(4)	3.7
			$11/2_1^-$	3393	52(16)			9(4)	28

[a]Reference [1].
[b]Present work.

TABLE VI. Experimental reduced transition probabilities $B(E1)$ compared to MCSM calculations performed using the SDPF-M interaction. The theoretical $B(E1)$ values have been obtained using effective electric charges of Ne/A and $-Ze/A$ for the proton and neutron, respectively.

E_x (keV)	τ (fs)	I_i^π	I_f^π	E_γ (keV)	BR (%)	$B(E1)(e^2\,\mathrm{fm}^2)$	
						Exp	SDPF-M
4431	600(100)[a]	$7/2_1^-$	$5/2_3^+$	240	0.7(2)	$5(2)\times10^{-4}$	7×10^{-5}
			$7/2_1^+$	1016	4.2(6)	$4(1)\times10^{-5}$	1×10^{-5}
			$5/2_2^+$	1136	43(3)	$3.1(5)\times10^{-4}$	5×10^{-5}
			$5/2_1^+$	2197	49(3)	$4.8(8)\times10^{-5}$	2×10^{-5}
6501	55(17)[a]	$9/2_1^-$	$7/2_1^+$	3086	16(2)	$6(2)\times10^{-5}$	1×10^{-4}
6796	202(42)[a]	$9/2_2^-$	$7/2_1^+$	3381	28(6)	$2.3(7)\times10^{-5}$	8×10^{-5}
6824	123(51)[a]	$11/2_1^-$	$9/2_1^+$	1481	40(3)	$6(3)\times10^{-4}$	5×10^{-5}
8705	230(40)[b]	$13/2_1^-$	$11/2_1^+$	2252	6(1)	$1.4(4)\times10^{-5}$	8×10^{-5}
9176	120(40)[b]	$13/2_2^-$	$11/2_2^+$	1734	12(4)	$1.2(6)\times10^{-4}$	1×10^{-4}
			$11/2_1^+$	2722	67(6)	$1.7(6)\times10^{-4}$	8×10^{-4}
9450	50(20)[b]	$13/2_3^-$	$11/2_3^+$	1106	2(1)	$2(1)\times10^{-4}$	1×10^{-3}
			$11/2_2^+$	2008	5(3)	$8(5)\times10^{-5}$	3×10^{-5}
10217	110(30)[b]	$15/2_1^-$	$13/2_1^+$	904	3(1)	$2(1)\times10^{-4}$	1×10^{-4}
10520	970(100)[b]	$15/2_1^+$	$13/2_3^-$	1070	25(4)	$1.7(3)\times10^{-4}$	1×10^{-4}
			$13/2_2^-$	1344	1.3(5)	$3(1)\times10^{-6}$	4×10^{-5}
			$13/2_1^-$	1815	59(7)	$6(1)\times10^{-5}$	1×10^{-4}
11297	1900(200)[b]	$17/2_1^+$	$15/2_2^-$	538	6(2)	$1.3(4)\times10^{-4}$	3×10^{-6}
			$15/2_1^-$	1080	25(7)	$7(2)\times10^{-5}$	$<10^{-6}$

[a]Reference [1].
[b]Present work.

IV. CONCLUSIONS

A detailed spectroscopic study of the $N = Z + 1$ nucleus ^{31}P, extended at high spin, has been done for the first time. Sixteen new levels have been observed up to an excitation energy of 13.9 MeV. Shell-model calculations performed using the code ANTOINE with the USD residual interaction and the Monte Carlo shell model with the SDPF-M interaction well reproduce the excitation energies and the reduced transition probabilities for positive-parity states with $I^\pi \leqslant 13/2^+$. The observed decay pattern and the measured lifetimes indicate a change of configuration at the $15/2^+$ and $17/2^+$ yrast states that is explained in terms of two particle-hole intruder excitations to the *fp* upper shell. The good description of the experimental data by MCSM calculations gives support to the validity of the adopted interaction in stable nuclei around ^{32}S.

ACKNOWLEDGMENTS

This work has been partly supported by the TMR European Contract No. HPRI-CT-1999-00083, by a Grant-in-Aid for Specially Promoted Research (13002001) from the MEXT (Japan), and by the RIKEN-CNS collaboration project on large-scale nuclear structure calculations. M.I.-B. and A.I. acknowledge partial support from the CERES Programme of the Romanian Ministry of Education and Research, Contract No. 3-11/2003-2005.

[1] P. M. Endt, Nucl. Phys. **A633**, 1 (1998), and references therein.
[2] J. Vernotte, G. Berrier-Ronsin, S. Fortier, E. Hourani, A. Khendriche, J. M. Maison, L.-H. Rosier, G. Rotbard, E. Caurier, and F. Nowacki, Nucl. Phys. **A655**, 415 (1999).
[3] B. A. Brown and B. H. Wildenthal, Annu. Rev. Nucl. Part. Sci. **38**, 29 (1988).
[4] H. Molique, J. Dobaczewski, and J. Dudek, Phys. Rev. C **61**, 044304 (2000).
[5] J. Zhang and W. D. M. Rae, Nucl. Phys. **A564**, 252 (1993).
[6] W. Satula and R. Wyss, Nucl. Phys. **A676**, 120 (2000).
[7] Y. Utsuno, T. Otsuka, T. Mizusaki, and M. Honma, Phys. Rev. C **60**, 054315 (1999).
[8] C. E. Svensson, E. Caurier, A. O. Macchiavelli, A. Juodagalvis, A. Poves, I. Ragnarsson, S. Åberg, D. E. Appelbe, R. A. E. Austin, C. Baktash, G. C. Ball, M. P. Carpenter, R. M. Clark, M. Cromaz, M. A. Deleplanque, R. M. Diamond, P. Fallon, M. Furlotti, A. Galindo-Uribarri, R. V. F. Janssens, G. J. Lane, I. Y. Lee, M. Lipoglavsek, F. Nowacki, S. D. Paul, D. C. Radford, D. G. Sarantites, D. Seweryniak, F. S. Stephens, V. Tomov, K. Vetter, D. Ward, and C. H. Yu, Phys. Rev. Lett. **85**, 2693 (2000).
[9] C. E. Svensson, A. O. Macchiavelli, A. Juodagalvis, A. Poves, I. Ragnarsson, S. Åberg, D. E. Appelbe, R. A. E. Austin, G. C. Ball, M. P. Carpenter, E. Caurier, R. M. Clark, M. Cromaz, M. A. Deleplanque, R. M. Diamond, P. Fallon, R. V. F. Janssens, G. J. Lane, I. Y. Lee, F. Nowacki, D. G. Sarantites, F. S. Stephens, K. Vetter, and D. Ward, Phys. Rev. C **63**, 061301(R) (2001).
[10] D. Rudolph, A. Poves, C. Baktash, R. A. E. Austin, J. Eberth, D. Haslip, D. R. LaFosse, M. Lipoglavsek, S. D. Paul, D. G. Sarantites, C. E. Svensson, H. G. Thomas, J. C. Waddington, W. Weintraub, and J. N. Wilson, Phys. Rev. C **65**, 034305 (2002).
[11] M. Ionescu-Bujor *et al.*, Annual Report 2000, LNL-INFN (REP)-178/2001, p. 6.
[12] M. Ionescu-Bujor *et al.*, Annual Report 2001, LNL-INFN (REP)-182/2002, p. 6.
[13] F. Della Vedova *et al.*, Annual Report 2004, LNL-INFN (REP)-204/2005, p. 7.
[14] F. Della Vedova, S. M. Lenzi, M. Ionescu-Bujor, N. Marginean, E. Farnea, M. Nespolo, G. de Angelis, M. Axiotis, D. Bazzacco, A. Bizzeti-Sona, P. G. Bizzeti, F. Brandolini, D. Bucurescu, A. Iordachescu, S. Lunardi, R. Menegazzo, D. R. Napoli, C. Rossi Alvarez, and C. A. Ur, AIP Conf. Proc. **764**, 205 (2005).
[15] P. Mason, N. Marginean, S. M. Lenzi, M. Ionescu-Bujor, F. Della Vedova, D. R. Napoli, T. Otsuka, Y. Utsuno, F. Nowacki, M. Axiotis, D. Bazzacco, P. G. Bizzeti, A. M. Bizzeti-Sona, F. Brandolini, M. A. Cardona, G. de Angelis, E. Farnea, A. Gadea, D. Hojman, A. Iordachescu, C. A. Kalfas, Th. Kröll, S. Lunardi, T. Martínez, C. M. Petrache, B. Quintana, R. V. Ribas, C. Rossi Alvarez, C. A. Ur, R. Vlastou, and S. Zilio, Phys. Rev. C **71**, 014316 (2005).
[16] C. Rossi Alvarez, Nucl. Phys. News **3**, 3 (1993).
[17] E. Farnea, G. de Angelis, M. De Poli, D. De Acuna, A. Gadea, D. R. Napoli, P. Spolaore, A. Buscemi, R. Zanon, R. Isocrate, D. Bazzacco, C. Rossi Alvarez, P. Pavan, A. M. Bizzeti-Sona, and P. G. Bizzeti, Nucl. Instrum. Methods Phys. Res. A **400**, 87 (1997).
[18] J. C. Wells and N. R. Johnson, Report No. ORNL-6689, 1991, p. 44.
[19] L. C. Northcliffe and R. F. Schilling, Nucl. Data, Tables A **7**, 233 (1970).
[20] P. M. Endt, At. Data Nucl. Data Tables **23**, 3 (1979).
[21] E. Caurier, ANTOINE code, Strasbourg, 1989.
[22] T. Otsuka, M. Honma, and T. Mizusaki, Phys. Rev. Lett. **81**, 1588 (1998).
[23] T. T. S. Kuo and G. E. Brown, Nucl. Phys. **A114**, 241 (1968).
[24] E. K. Warburton, D. E. Alburger, J. A. Becker, B. A. Brown, and S. Raman, Phys. Rev. C **34**, 1031 (1986).
[25] D. J. Millener and D. Kurath, Nucl. Phys. **A255**, 315 (1975).
[26] Y. Utsuno, T. Otsuka, T. Glasmacher, T. Mizusaki, and M. Honma, Phys. Rev. C **70**, 044307 (2004).